A Coupled CFD-Monte Carlo Method for Simulating Complex Aerosol Dynamics in Turbulent Flows

Shuyuan Liu[1] and Tat Leung Chan[1,2,*]

[1]Department of Mechanical Engineering, The Hong Kong Polytechnic University, Kowloon, Hong Kong

[2]The Hong Kong Polytechnic University Shenzhen Research Institute, Shenzhen, PR China

Abstract

A coupled computational fluid dynamics (CFD)-Monte Carlo method is presented to simulate complex aerosol dynamics in turbulent flows. A Lagrangian particle method based probability density function (PDF) transport equation is formulated to solve the population balance equation (PBE) of aerosol particles. The formulated CFD-Monte Carlo method allows investigating the interaction between turbulence and aerosol dynamics and incorporating individual aerosol dynamic kernels as well as obtaining full particle size distribution (PSD). Several typical cases of aerosol dynamic processes including turbulent coagulation, nucleation and growth are studied and compared to the sectional method with excellent agreement. Coagulation in both laminar and turbulent flows is simulated and compared to demonstrate the effect of turbulence on aerosol dynamics. The effect of jet Reynolds (Re_j) number on aerosol dynamics in turbulent flows is fully investigated for each of the studied cases. The results demonstrate that Re_j number has significant impact on a single aerosol dynamic process (e.g. coagulation) and the simultaneous competitive aerosol dynamic processes in turbulent flows. This newly modified CFD-Monte Carlo/PDF method renders an efficient method for simulating complex aerosol dynamics in turbulent flows and provides a better insight into the interactions between turbulence and the full PSD of aerosol particles.

Keywords: aerosol dynamics, computational fluid dynamics (CFD), Monte Carlo method, population balance, turbulent flows

1. Introduction

Turbulent flows with complex aerosol dynamics of polydispersed particles are encountered in many scientific and engineering problems. Examples mainly include the exhaust particle formation and evolution in the wake of the studied ground vehicle (Chan et al., 2010), the dynamics and dispersion of nanoparticles in urban atmospheric environment (Yu and Chan, 2009; Kumar et al., 2011), the nanoparticle synthesis in turbulent reacting flows (Yu et al., 2008; Akroyd et al., 2011), and the formation of soot particles in combustion engines (Chan and Cheng, 2007; Cenker et al., 2013; Pang et al., 2016). Particles involved in the aerosol processes are characterized by a polydispersed particle size distribution (PSD). The control over PSD of the particles in turbulent flows is of paramount significance in many industrial and engineering applications because PSD reveals the basic properties of product particles or emission particles, which in turn determines the engineering application or environmental effect. The PSD is subject to turbulent flow field besides the complex aerosol dynamics that particles are involved.

*Corresponding author: Tat Leung Chan, E-mail address: mmtlchan@polyu.edu.hk

Population balance equation (PBE) is used to describe the evolution of PSD of particles mathematically (Ramkrishna, 2000), which is a transport equation of particle number density function dependent on space coordinates, time and particle size. Depending on actual aerosol dynamic processes, different source terms such as coagulation, nucleation and growth may appear in PBE, as shown in Equation (4) of Section 2.1. Combining different source terms into different physical processes, the PBE (i.e., in Equation (4)) is obviously an integro-differential equation. There has been a large number of research studies concerning the solution of PBE in spatially homogeneous domain i.e., zero dimensional PBE (Efendiev, 2004; Yu et al., 2009; Chan et al., 2010; Zhou and Chan, 2011; Geng et al., 2013; Yu and Chan, 2015; Liu et al., 2015).

However, in actual industrial and engineering applications, an inhomogeneous flow field is generally encountered which has a profound impact on aerosol dynamic processes. Those processes are basically dependent on local flow field variables (e.g., temperature, concentration). Thus the solution for multidimensional PBE including convection term and diffusion terms becomes significant for aerosol dynamics in turbulent flows. Coupling the PBE of aerosol dynamics with CFD method provides a very promising approach to deal with the spatially inhomogeneous problems of aerosol dynamics (Kruis et al., 2012; Zhao and Zheng, 2013; Zhou and Chan, 2014; Zhou and He, 2014; Akridis and Rigopoulos, 2015; Amokrane et al., 2016). In laminar flow, the coupling of CFD to PBE can be easily accomplished via proper transformation of PBE. However, in turbulent flows, the closure problems arise due to the effect of turbulence on aerosol dynamic processes (e.g. coagulation, nucleation and growth) as such physical processes are highly dependent on the local field variables. Moreover, the relationship between turbulence, particle properties and collision kernels of aerosol dynamics is not well understood due to the theoretical limitations and experimental difficulties (Reade and Collins, 2000; Balachandar and Eaton, 2010**)**. Thus particular attention is paid to examine the effect of turbulence on aerosol dynamics and the evolution of PSD of aerosol dynamics in the present study.

Probability density function (PDF) methods based on a PDF transport equation have been proposed and used to deal with turbulence, scalar transport or combustion problems in turbulent reactive flows for more than three decades (Pope, 1981; Pope, 1985; Valino, 1998; Sabel'nikov and Soulard, 2005; Meyer, 2010; Pope and Tirunagari, 2014; Consalvi and Nmira, 2016). Originated mainly from the work of Lundgren (1967), the PDF approach has then been improved and extended by many eminent researchers. Monte Carlo methods for solving the joint scalar and velocity-scalar PDF were developed by Pope (1981, 1985) and were reviewed comprehensively in the book by Fox (2003). The PBE-PDF transport equation was firstly derived in Rigopoulos (2007), and the CFD-Lagrangian Monte Carlo method was also firstly proposed and developed in Di Veroli and Rigopoulos (2010, 2011), based on which the CFD-Lagrangian Monte Carlo method is further modified in the present study. Both PSD and particle number density distribution can then be treated without additional assumptions for closure via the transported PDF methods. The full PSD can thus be obtained directly with the transported PDF methods. The work of Di Veroli and Rigopoulos (2010) was the first paper to develop a Lagrangian Monte Carlo method for the PDF of the PSD for a reactive precipitation problem and this method was used on an aerosol condensation problem in Di Veroli and Rigopoulos (2011). The concept was applied to LES in Pesmazoglou et al. (2014) and to deal with aggregation in Pesmazoglou et al. (2016). Moreover, complex and arbitrary kernels of aerosol dynamics are allowed since no closure is required for the PBE. These PDF methods can be divided into three categories i.e. Eulerian particle method (Pope, 1981), Lagrangian particle method (Pope, 1985) and Eulerian field method (Sabel'nikov and Soulard, 2005). Both the advantages and disadvantages of the methods and possible improvements can easily be identified in the comparison between Eulerian and Lagrangian Monte Carlo PDF methods (Mobus et al., 2001; Zhang and Chen, 2007; Jaishree and Haworth, 2012).

Lagrangian particle Monte Carlo algorithms (Pope, 1985) have been regarded as the mainstream approach for solving PDF transport equations in most applications of PDF methods to date (Jaishree and Haworth, 2012). The PDF is represented by a great number of notional particles which evolve according to the prescribed stochastic differential equations (SDE), and weighted averages over the particles in a small amount of neighboring grids are used to approximate the local mean quantities. As the mean velocity and turbulence are required for before advancing in every time step, it is necessary to couple the Lagrangian particle method with a conventional CFD solver to formulate a hybrid Lagrangian particle/Eulerian mesh PDF method (Jaishree and Haworth, 2012). The main advantage of Lagrangian particle method relative to Eulerian PDF method is that the spatial-transport algorithm has much higher accuracy. The number of grid cells required for equivalent accuracy is thus considerably smaller and the total computational cost of Lagrangian PDF is only proportional to the number of notional particles despite of the special care required for reducing statistical error. In the present study, a newly modified consistent hybrid Lagrangian particle/Eulerian mesh PDF method based mainly on the work of Rigopoulos (2007) is presented for the coupled CFD-Monte Carlo simulation of aerosol dynamics in turbulent flows. The novelty of the present study is to investigate the effect of Re_j number on the PSD of typical aerosol dynamic processes in turbulent flows. The enhancing effect of turbulence on aerosol dynamic processes as well as the competition and transition between different aerosol dynamic processes are noted and analyzed. A new particle tracking method with high computational efficiency is adopted in the Monte Carlo simulation. Moreover, the operator splitting technique recently proposed by Liu and Chan (2016) for solving simultaneous aerosol dynamic processes is also used to increase the computational efficiency and accuracy.

2. Methodology

2.1. Governing equations

The governing equations of the coupled fluid-particle dynamics in incompressible flows include the continuity and momentum equations i.e. Navier-Stokes equations (1) and (2) as well as species transport equation i.e. Eq. (3) (Rigopoulos, 2007).

$$\nabla \cdot u\,(x, t) = 0 \tag{1}$$

$$\partial u\,(x, t)/\partial t + (u\,(x, t)\cdot\nabla)u\,(x, t) = \nu\nabla^2 u\,(x, t) - \nabla P\,(x, t)/\rho \tag{2}$$

$$\partial Y_a/\partial t + \nabla(u\,(x, t)\cdot Y_a) = D_a\nabla^2 Y_a + \dot{\omega}(Y_1, Y_2, \ldots, Y_m) \tag{3}$$

where u is the velocity of the carrier fluid phase, ν is the kinematic viscosity which is assumed constant, x is the coordinates of particles, t is the time, P is the pressure, ρ is the fluid density, Y_a is the mass fraction of species (i.e., a= 1, 2,…, m), D_a is the diffusion coefficient in composition space and $\dot{\omega}$ is the source term determined by the aerosol dynamic processes (i.e., coagulation, nucleation and growth) in the present study. An in-house time dependent Reynolds Averaged Navier Stokes (RANS) code and k-ε turbulence model are used together with the following transported PDF method. More detailed information about the in-house CFD code can be found in Section S1 of the online supplementary information (SI) file of this paper.

The PBE in terms of particle number density $n(v, x, t)$, a function of particle volume as well as of space coordinates and time, can be written as Equation (4), in which $n(v, x, t)$ is written as $n(v)$ for simplicity,

$$\partial n(v)/\partial t + \nabla(\boldsymbol{u}\cdot n(v)) + \partial(G(Y_1, Y_2,\ldots,Y_m, v)\cdot n(v))/\partial v$$
$$= D_p\nabla^2 n(v) + B(Y_1, Y_2,\ldots,Y_m, v)\cdot\delta(v - v_0)$$
$$+ 1/2\int_{v_0}^{v-v_0} K(u, v-u)n(u, t)n(v-u, t)\mathrm{d}u - n(v,t)\int_0^{\infty} K(u, v)n(u, t)\mathrm{d}u \quad (4)$$

The terms in PBE i.e. Equation (4) from the left-hand side to the right-hand side are:

- Accumulation term of the particle number density.
- Convection term in physical space, $\boldsymbol{u}$ is the velocity of carrier fluid phase.
- Condensation/growth term in phase space, where $G(Y_1, Y_2,\ldots,Y_m, v)$ is the growth kernel, Y_m is the function species concentration, m is the number of species and v is the particle volume.
- Particle diffusion term, where D_p is the diffusion coefficients of particles.
- Nucleation term, where $B(Y_1, Y_2,\ldots,Y_m, v)$ is the nucleation kernel, Y_m is the function species concentration and v is the particle volume. This term contributes a source for particle with the size of v_0 which is the minimum particle size of the nuclei.
- Coagulation term, which consists of two parts. The first part is the birth part accounting for all the possible gains in particle number density with size of v due to the coagulation between particle of size (v-v_0) and v_0. The factor 1/2 is used to prevent double counting the coagulation events. The second part is the death part accounting for all the loss of particles with size of v due to all the possible combinations. $K(u,v)$ is the coagulation kernel dependent on the size of colliding pairs.

2.2. PDF transport equation formulation

The derivation of PDF formulation for aerosol dynamics in turbulent flows is based on the work of Rigopoulos (2007). First of all, a joint multipoint PDF of the mass concentration and particle number density of species at full size range is introduced so that the expected PSD at any point can be determined:

$$Y(\boldsymbol{x}, t),\ n(v, \boldsymbol{x}, t) \equiv f(Y, N; \boldsymbol{x}, t) \quad (5)$$

where $Y \equiv y_1, y_2, \ldots, y_m$ and $N \equiv n_1, n_2, \ldots, n_n$ have the following constraints:

$$y_a < Y_a(\boldsymbol{x}, t) < y_a + dy$$
$$n < N(v_i, \boldsymbol{x}, t) < n + dn \quad (6)$$

and the normalization property is also satisfied:

$$\int_0^1\int_0^{\infty} f(Y, N; \boldsymbol{x}, t)\mathrm{d}Y\mathrm{d}N = 1 \quad (7)$$

2.2.1. Discretization of the continuous PBE

As the continuous function of $n(v, \boldsymbol{x}, t)$ is needed for the source terms (e.g. the nucleation growth/condensation and coagulation), the continuous PBE is discretized based on the approximation of infinite space points with finite space points (Rigopoulos and Jones, 2003):

$$N(v) \approx \{N(v_1), N(v_2),\ldots, N(v_n)\} = \{N_1, N_2,\ldots, N_n\} \tag{8}$$

The discretized form of PBE can be written as:

$$\begin{aligned} &\partial N_i/\partial t + \nabla(u\cdot N_i) + G_1(Y)\cdot N_i + G_2\cdot N_{i-1} \\ &= D_p\nabla^2 N_i + B_1(Y) + 1/2\sum_{j=1}^{i-1} a_{i\text{-}j,j}(v_{i\text{-}j}, v_j)\cdot N_{i\text{-}j}N_j - N_i\sum_{j=1}^{n} a_{i,j}(v_i, v_j)\cdot N_j \end{aligned} \tag{9}$$

where N is the set of particle number density, u is the velocity of carrier fluid phase, G_1 and G_2 are the growth kernels, $a_{i\text{-}j,j}$ and $a_{i,j}$ are the coagulation kernels and v is the particle volume. More details about the discretization of the continuous PBE can be found in Section S3 of the online SI file of this paper.

2.2.2. Final PDF transport equation

Based on full derivations in Rigopoulos (2007), the final transport equation of PDF is expressed as follows:

$$\begin{aligned} \frac{\partial f}{\partial t} = &-\bar{u}\cdot f - <u'\nabla F> - \sum_{a=1}^{m}\sum_{b=1}^{m} D\frac{\partial^2(\nabla Y_a\cdot\nabla Y_a\cdot F)}{\partial y_a\partial y_b} \\ &-\sum_{i=1}^{n}\sum_{j=1}^{n} D_p\frac{\partial^2(\nabla N_i\cdot\nabla N_i\cdot F)}{\partial n_i\partial n_j} - \frac{\partial}{\partial y_a}[B_1(y_1, y_2,\ldots,y_m)\cdot f] \\ &+\frac{\partial}{\partial n_i}[(G_1(y_1, y_2,\ldots,y_m)n_i - G_2\cdot n_{i\text{-}1})\cdot f] \\ &-\sum_{i=1}^{n}\frac{\partial}{\partial n_i}[1/2\sum_{j=1}^{i\text{-}1}(a_{i,j}\cdot n_{i\text{-}j}n_j)\cdot f] + \sum_{i=1}^{n}\frac{\partial}{\partial n_i}[n_i\sum_{i=1}^{n}[(a_{i,j}\cdot N_j)\cdot f] \end{aligned} \tag{10a}$$

$$F = \prod_{a=1}^{M}\delta(Y_a - y_a)\cdot\prod_{i=1}^{N}\delta(N_i - n_i) \tag{10b}$$

where $\bar{u}\cdot f$ and $<u'\nabla F>$ are the convection terms in physical space due to mean velocity field and turbulent transport, respectively, f is the joint composition PDF of particles and equals to $<F>$, $a_{i,j}$ is the coagulation kernel, m is the number of species and F is a fine-grained density (Lundgren, 1967).

2.3. Monte Carlo simulation

The Monte Carlo method developed by Pope (1981, 1985) is further extended to solve the PDF transport equation of aerosol dynamics in turbulent flows. The underlying concept of this Monte Carlo method is to simulate a number of stochastic entities, whose evolution statistics obtained via stochastic differential equations as well as CFD method approximate the PDF of interest. The stochastic model for the evolution of particle position and particle number density used to advance PDF is as follows (Di Veroli and Rigopoulos, 2010):

$$X^n(t+\Delta t)=X^n(t)+[<U>(X^n(t),t)+\nabla\Gamma_T(X^n(t),t)]\Delta t+[2\Gamma_T(X^n(t),t)]^{1/2}\Delta W \tag{11}$$

$$N^n(t+\Delta t)=N^n(t)+[C_N/2(<N^n(t)>-N^n(t))+\dot{W}_i(N,Y)]\Delta t \tag{12}$$

where ΔW_i is a Gaussian pseudo-random number for representing the stochastic fluctuations of Wiener process with mean $<\Delta W_i>=0$ and covariance $<\Delta W_i \Delta W_j>=\Delta t\delta_{i,j}$, C_N is the characteristic scale concerning micro mixing, $\dot{W}_i(N,Y)$ is the source term for accounting the variation of particle number density, Γ_T is the turbulent diffusion coefficient, $<U>$ is the average velocity.

It is noteworthy that a new particle tracking method is used in the simulation of coagulation events of particles. Instead of looping several neighboring grid cells which contain a large amount of notional particles, the loop checking will be carried out within only one grid cell. It implies that the loop checking will be performed over all the particles located within the grid cell to counter check if they are involved in coagulation events. The possible grid cell in which the tracked particles may be located after a time step, Δt is determined before sorting its possible coagulation partners. Then Monte Carlo method is applied to determine the probability of certain aerosol dynamic events in the certain grid cell. It is reasonably assumed that all the coagulation events within one time step, Δt of a tracked notional particle take place in one same grid cell. By this assumption, the computational time spent on sorting particles for coagulation is greatly reduced, thus increasing the computational efficiency. The operator splitting technique of second-order accuracy in Liu and Chan (2016) is used to deal with the intra-cell simultaneous aerosol dynamic processes. The operator splitting technique separates the integration into multiple steps rather than integrates all the aerosol dynamic processes together in a single step. The implementation procedures of the present modified Lagrangian PDF approach based CFD-Monte Carlo method can be found in Section S2 of the online SI file of this paper.

2.4. Simulation analysis

In order to analyze the variation of particle number density along the axial distance, the particle number density is sampled at different evenly distributed positions in the axial direction with the interval of 0.125 m. The normalized particle number density is defined as the ratio of local particle number density to the particle number density at the outlet of the nozzle as follows:

$$N_n = N_l / N_0 \tag{13}$$

where N_n is the normalized particle number density, N_l is the local particle number density in the computational domain and N_0 is the particle number density at the outlet of the nozzle.

3. Numerical simulation setup

The configuration of the aerosol reactor in the present study is shown in Fig. 1. The aerosol reactor is a cylindrical aerosol reactor with radius of 0.225 m and length of 2 m. A nozzle with radius of 0.005m and length of 0.01 m is located at the center of the cylindrical aerosol reactor. Three partitions with height of 0.05 m and thickness of 0.0005 m are evenly mounted in the axial direction inside the cylindrical aerosol reactor in order to enhance mixing. For aerosol dynamics in turbulent flows, particles with a volume fraction of 0.1 in the carrier gas (air) is injected from the nozzle while gas phase (air) is injected through the gas phase inlet. The injected particles are potassium chloride (KCl) particles with a size range of 0.1 μm to 6.4 μm and density of 1980 kg/m^3 (Calvo et al., 2013). The injection velocity of particulate phase ranges from 10 m/s to 40 m/s, the inlet velocity of gas phase is 0.5 m/s. Coagulation kernel is obtained using the turbulent coagulation model by Saffman and Turner (1956). The nucleation rate is kept constant at 7.5×10^6 /m^3·s with constant growth rate of 6.2×10^{-11} m/s. Aerosol dynamics in laminar flow is also investigated in the same aerosol reactor for comparison with aerosol dynamics in turbulent flows, which is carried out by switching the inlet conditions of velocity and species between the inlets of the nozzle and the gas phase. Specifically, for the study of aerosol dynamics in the laminar flow, particles enter the gas phase inlet instead of the nozzle as shown in Fig. 1 while the nozzle is used for the entry of air at a low velocity of 0.5 m/s.

FIG.1. Three-dimensional schematic configuration of a cylindrical aerosol reactor (Two-dimensional axisymmetric grid is generated in the rectangular domain ABCD, not in scale).

Four injection velocities of particulate phase i.e. 10 m/s, 15 m/s, 20 m/s and 40 m/s are used to investigate the effect of jet Reynolds (Re_j) number on the aerosol dynamics in turbulent flows. The turbulent kinetic energy distributions in the aerosol reactor can be found in Section S5 of the online SI file of this paper. Temperature is kept at 300 K for all the computational domain. The standard k-ε turbulence model is used for the turbulence computation. After balancing the computational accuracy and cost, 30 notional particles are allocated in each cell in the present Monte Carlo simulation. The simulation parameters for aerosol dynamics in turbulent flows are summarized in Table 1. The computational grid of the present coupled CFD-Monte Carlo method can be found in Fig. S1 of the online SI file of this paper.

Table 1. Simulation parameters for aerosol dynamics in turbulent flows.

4. Results and discussion

4.1. Coagulation in laminar and turbulent flows

As mentioned above in Section 3, the inlet of fluid and particulate phases is switched to simulate laminar flow, i.e. the particles are injected into the aerosol reactor through the air inlet while air is injected through the nozzle (as shown in Fig. 1). The Re_j number at the nozzle is 3200 with the injection velocity of 10 m/s for turbulent flows. The entry velocity of the gas phase (air) is 0.5 m/s for both cases.

Fig. 2 shows the initial PSD of particles before entering the aerosol reactor. It can be seen that small particles account for the majority of the total particle population. Fig. 3 shows the PSD for particles after coagulation in

both laminar and turbulent flows. Compared with the PSD in Fig. 2, it can be seen that the PSD in Fig. 3 varies significantly in its shape and order of magnitude (decreasing from the magnitude of 10^{19} to 10^{16}) due to coagulation. Coagulation is obviously enhanced in turbulent flows which can be seen from the wider spectrum of PSD and higher maxima of particle number density when compared to that in laminar flow. This is because coagulation in an inter-particle process is dependent on the concentration and the mixing effect of particles. Enhanced coagulation leads to a higher number density of particles with diameter of 0.6 μm. As coagulation is just enhanced and the coagulation mechanism is not changed, the peaks of the PSDs for laminar and turbulent coagulation processes in Fig. 3 appear in the same particle size.

FIG. 2. Initial PSD before entering the aerosol reactor.

FIG. 3. PSD in laminar and turbulent coagulation.

Fig. 4 shows the particle number density distribution within the same aerosol reactor for laminar and turbulent flows, respectively. As particle number density decreases during pure coagulation process, the coagulation rate distribution can be characterized by the particle number density distribution within the reactor. From Fig. 4(a), the high particle number density regions can be found throughout the first half of the reactor in laminar flow which implies low coagulation rates in these regions. The particle number density does not decrease significantly until the second half of the reactor. It suggests that coagulation mainly takes place in the second half of the reactor, which renders high particle number density and low average coagulation rate throughout the whole reactor in laminar flow. It can be seen from Fig. 4(b), however, the particle number density in turbulent flows remains very low in most of the regions within the aerosol reactor except for some zones near the outlet of the aerosol reactor and behind the partitions. It demonstrates that coagulation process is obviously enhanced in turbulent flow compared to coagulation in laminar flow.

FIG. 4. Particle number density (#/m^3) contour in laminar and turbulent coagulation.

4.2. Coagulation in turbulent flows

The effect of Re_j number on coagulation process in turbulent flows is further studied. Varied jet velocities of 10 m/s, 15 m/s, 20 m/s and 40 m/s are used with corresponding *Re* numbers of 3200, 4800, 6400 and 12800, respectively. The results obtained via the present modified Lagrangian Monte Carlo/PDF (LMC-PDF) method are directly compared with that obtained with the population balance sectional method (PBSM) (Hounslow et al., 1988).

Fig. 5 shows the obvious effect of different Re_j numbers on the PSD of aerosol particles experiencing coagulation process in turbulent flows. With *Re* number of the jet increasing from 3200 to 12800, the PSDs become wider and higher, with the peaks moving towards the larger end of particle size range, which yields a more evenly distributed population of particles. By controlling proper turbulent flow field, the control over PSD of aerosol particles can be achieved, which is of importance in industrial and engineering applications. Comparing the results obtained with the present modified LMC-PDF method and PBSM (Hounslow et al., 1988), an excellent agreement can be observed, which validates the reliability and computational efficiency of this modified LMC-PDF method. The wider PSD with increasing Re_j number is also in accordance with the previous research studies by Reade and Collins (2000) and Garrick (2015), which reveals the effect of turbulence on PSD. By increasing

Re_j numbers, turbulence induced mixing is greatly enhanced, which leads to an enhanced coagulation process. Meanwhile, the peaks of PSD moving towards the upper end of particle size spectrum with increasing Re_j number implies that more and larger particles are produced by enhanced coagulation. In other words, as coagulation is enhanced, larger particles have a better chance to appear due to more frequent collisions.

FIG. 5. PSD in turbulent coagulation: Case A, Re_j=3200; Case B, Re_j=4800; Case C, Re_j=6400; Case D, Re_j=12800 (The PBSM results are obtained based on the method proposed by Hounslow et al., 1988).

According to the definition of particle number based average diameter of particles (Friedlander, 2000), the number averaged particle diameter can be obtained by integrating the PSD over the entire particle diameter range and then averaging over the total particle number density of particles. Using this method, the initial average diameter and average diameters of particles under the turbulent coagulation with different Re_j numbers are obtained and shown in Fig. 6. An increase in average diameter from 0.124 μm to 0.245 μm can be observed with increasing *Re* number from 0 to 12800, which is an obvious increase considering the large number of aerosol particles in the aerosol reactor. The Re_j number of 0 corresponds to the initial PSD of aerosol dynamics before entering the aerosol reactor. As higher Reynold number of the jet is related to higher turbulent intensity in the present study**,** the increase of average diameter with Re_j number indicates that coagulation is significantly enhanced, which may be explained by the enhanced mixing and more frequent collisions between particles.

FIG. 6. Average diameter of particles for different aerosol dynamic processes in turbulent flows.

The particle number density (m^{-3}) contour in turbulent coagulation under different Re_j number is shown in Fig. 7. It can be seen that despite of the similar distribution pattern of particle number density in the reactor, the particle number density decreased with increasing Re_j number due to coagulation, which suggests an increase in average coagulation rate with the increase of Re_j number. Fig. 8 shows the variation of normalized particle number density with the axial distance under different Re_j numbers. As coagulation process continuously reduces particle number density, it can be seen that the normalized particle number density for any given Re_j number decreases with the axial distance as coagulation process takes place. Consider the same axial position, the difference between the normalized particle number density shows the different coagulation rates. Obviously, a higher Re_j number yields higher turbulence, which in turn leads to a higher coagulation rate. The results in Fig. 8 show clearly the enhancing effect of turbulence on coagulation. When Re_j number reaches 12800, the maximum value used in the present study, it can be observed that the normalized particle number density first decreases rapidly, then decreases slightly and finally decreases with the rate almost equal to that with Re_j number of 6400. The three-stage decrease of normalized particle number density indicates that the coagulation rate experiences with three different stages. This may be explained by the physical nature of coagulation process. Coagulation is a binary particle event which is dependent on local concentration of particles and micro-mixing. Coagulation rate is first increased due to the enhanced mixing caused by high turbulence, which consumes a large number of particles in a short time. As a result, a low local concentration of particles in turn reduces the coagulation rate until more particles are accumulated and coagulation rate increases again in the final stage.

FIG. 7. Particle number density (#/m^3) contour in turbulent coagulation.

FIG. 8. Normalized particle number density in turbulent coagulation.

4.3. Coagulation and nucleation in turbulent flows

The effect of different Re_j numbers on two simultaneous aerosol dynamic processes (i.e. coagulation and nucleation) in turbulent flows is studied. The adopted Re_j numbers are the same as described before. Coagulation process is modeled by the turbulence model used in Saffman and Turner (1956) while nucleation rate is kept constant as $7.5\times10^6/m^3\cdot s$ for all the studied cases. Also, the results are validated with the PBSM (Hounslow et al., 1988).

The PSD of turbulent coagulation and nucleation for different Re_j numbers is shown in Fig. 9. Compared with the PSD shown in Fig. 5, in which only coagulation is involved, the PSDs presented in Fig. 9 become much more complicated due to the simultaneous coagulation and nucleation processes in turbulent flows. For the case with Re_j number of 3200, the PSD extends throughout the full particle size range with peaks falling into both small size range (less than 1 μm) and large size range (larger than 2 μm), which suggests that the simultaneous nucleation and coagulation processes taking place and producing small particles and relatively large particles simultaneously. As Re_j number increases from 3200 to 4800, a new peak appears on the new PSD whose position is around 2.5 μm while the other part of the PSD only varies slightly. It indicates that coagulation process is enhanced, which produces relatively larger particles to some extent. However, as Re_j number increases from 4800 to 6400, a new peak appears at the position of 1μm on the PSD while the other part of the PSD remains basically the same. It is probably because nucleation process is enhanced. With further increase of Re_j number from 6400 to 12800, the shape of PSD and the positions of peaks both remain unchanged, but the values of the peaks are greatly increased, which implies the competition between coagulation and nucleation is not changed. With Re_j number increases from 4800 to 6400 and up to 12800, a transition from coagulation-dominant mechanism to competitive co-existence of coagulation and nucleation can be reasonably concluded from Fig. 6. According to Garrick (2015), nucleation is the dominant process until the collapse of the jet potential core and turbulent mixing begins in the proximal region of the jet, where coagulation becomes the dominant process and leads to a broader PSD. Although increasing Re_j number may lead to stronger turbulence in order to enhance coagulation, high velocity of jet also causes the delay of turbulent mixing in which nucleation becomes dominant in the proximal region of the jet. The reason accounting for the change of PSD mentioned above can be verified by the evolution of average diameter of particles with increasing Re_j number as shown in Fig. 6. It can be seen that the average diameter of particles increases slightly with increasing Re_j number from 3200 to 4800, and reaches the peak of around 0.8 μm on the PSD. This is due to the enhanced coagulation as nucleation leads to smaller average diameter of particles. Moreover, Fig. 6 shows that average diameter of particles decreases when Re_j number is larger than 4800, which yields a maximum average diameter of particles at $Re_j = 4800$ for these four studied cases. The Re_j number at zero corresponds to the initial average diameter of particles before entering into the aerosol reactor.

FIG. 9. PSD for simultaneous coagulation and nucleation in turbulent flows: Case A, Re_j=3200; Case B, Re_j=4800; Case C, Re_j=6400; Case D, Re_j=12800 (The PBSM results are obtained based on the method proposed by Hounslow et al., 1988).

The contour of particle number density for simultaneous coagulation and nucleation is shown in Fig. 10. With Re_j number increasing from 3200 to 4800, the maxima of the particle number density decreases from 8.61×10^{16} m^{-3} to 5.76×10^{16} m^{-3}, implying that coagulation process which reduces particle density is dominant. An increase of the maxima of particle number density from 5.76×10^{16} m^{-3} to 7.42×10^{16} m^{-3} is observed when Re_j number increases from 4800 to 12800. Comparing Fig. 10 with Fig. 6, it can be found that the variation particle

number density contour is consistent with the variation of average particle diameter, which reflects the fact that coagulation becomes dominant with Re_j number increasing from 3200 to 4800. However, as Re_j number increases from 4800 to 6400 and then up to 12800, nucleation becomes dominant in the competition with coagulation as the average diameter decreases continuously.

FIG. 10. Particle number density (#/m^3) contour for simultaneous coagulation and nucleation in turbulent flows.

Fig. 11 shows the variation of normalized particle number density with axial distance. It can be seen clearly that the normalized particle number density experiences significant change with Re_j number increasing from 3200 to 4800 and up to 12800. The normalized particle number density increases rapidly with Re_j number of 3200, which implies that nucleation is the dominant mechanism resulting in a large number of new particles. As Re_j number increases from 3200 to 4800, the normalized particle number density decreases significantly, indicating that the dominant mechanism in the aerosol reactor changes from nucleation to coagulation as the latter reduces the total number of particles, which is also in accordance with the increase of average particle diameter as shown in Fig. 6. However, as the Re_j number further increases from 4800 to 6400 and up to 12800, the normalized particle number density also increases when compared with Re_j number of 4800 at the same axial position. These results indicate that coagulation is weakened while nucleation is enhanced when Re_j number increases from 4800 up to 12800, which is consistent with the findings in Garrick (2015) that too high injection velocity causes the delay of turbulent mixing and in turn reduces coagulation rate as mentioned above.

FIG. 11. Normalized particle number density for simultaneous coagulation and nucleation in turbulent flows.

4.4. Coagulation, nucleation and growth in turbulent flows

Complex aerosol dynamics in turbulent flows has been widely encountered and is a challenging problem in the numerical research. The PSDs of aerosol particles experiencing simultaneous coagulation, nucleation and growth processes under different Re_j numbers are shown in Fig. 12. The results are also validated with PBSM (Hounslow et al., 1988). Comparing with the results of PSDs in Fig. 9, it can be found that the shape of the PSDs are basically the same except for the positions and values of some peaks on them. The PSD at Re_j = 3200 is also characterized by its peaks, which are closer to the lower end of the particle size range when compared to that in Fig. 9. The different positions of peaks of the PSD should be due to the growth process since the other conditions in this case are the same with that in turbulent coagulation and nucleation process except that growth process is introduced. With Re_j number increasing from 3200 to 4800, a new peak at around 1.5 μm appears on the new PSD. This is caused by the growth and coagulation processes as nucleation process forms much smaller particles rather than particles with diameter of 1.5 μm, which is shown by the increase of average particle diameter with Re_j number increasing from 3200 to 4800 in Fig. 6. However, as Re_j number increases from 4800 to 6400, the value of the peak at 1.5 μm decreases very slightly while the value of the peak at around 0.6 μm increases significantly, which may be due to the enhanced nucleation process as nucleation produces more particles with the smallest size. The value of the peak at 0.6 μm increased sharply again with Re_j number increasing from 6400 to 12800, implying that nucleation process is further enhanced to be the dominant process.

FIG. 12. PSD for simultaneous coagulation, nucleation and growth in turbulent flows: Case A, Re_j=3200; Case B, Re_j=4800; Case C, Re_j=6400; Case D, Re_j=12800 (The PBSM results are obtained based on the method proposed by Hounslow et al., 1988).

The average diameters of particles for different Re_j numbers are calculated in order to reveal the physical mechanism behind the change of the PSD. Fig. 6 shows an increase in average diameter for increasing Re_j number from 3200 to 4800. Whereas for Re_j number larger than 4800 (within these four studied Re_j numbers for this case), the average diameter of particles decreases with increasing *Re* number. Based on the average diameter of particles calculated from the obtained PSD, it can be concluded that, with increasing Re_j number from 4800 to 6400, the change of the peak at around 0.6 μm is due to pure nucleation as neither growth nor coagulation leads to the decrease in average diameter. Comparing the case of turbulent coagulation and nucleation with this case in, it can be found that the particle number density of small particles increases with Re_j number in both of the two cases, which implies that nucleation is the dominant process among the simultaneous processes in the present study.

Fig. 13 shows the particle number density contour for simultaneous coagulation, nucleation and growth in turbulent flows. Consistent with the variation of average diameter of particles, the maxima of the particle number density contour also increases with increasing Re_j number from 3200 to 4800 and then decreases with Re_j number for larger than 4800. The variation of particle number density contour also verifies the effect of Re number on the competition between coagulation and nucleation. The dominant process changes from coagulation to nucleation with increasing Re_j number from 3200 to 128000 in the present study. Comparing with the results in Fig. 10, regions with high particle number density appear within the core of the jet in Figs. 13(a) to (c), which may be due to the growth processes taking place in these regions. The high particle number density regions in Fig. 13(d), however, move from the core of the jet/ nozzle injection to the zone between the second and the third partitions, and close to the wall of the aerosol reactor. This may be because this zone becomes a dead zone of flow and mixing for Re_j = 12800, which leads to weakened coagulation process in this dead zone of flow and mixing.

FIG. 13. Particle number density (#/m^3) contour for simultaneous coagulation, nucleation and growth in turbulent flows.

Fig. 14 presents the variation of normalized particle number density with the axial distance. It can be seen that the variation of normalized particle number density is basically the same for all the four studied Re_j numbers despite small differences, which increases first until a peak appears between the second and the third partitions of the aerosol reactor. Except for the case with Re_j number of 12800, the normalized particle number density after the peak decreases, and then basically remains stable with slight increase at the outlet of the aerosol reactor for all the other three studied cases. The variation of normalized particle number density for Re_j number ranging from 3200 to 6400 can be explained by the competition of multiple aerosol dynamic processes including coagulation, nucleation and growth. However, the particle number density at the peak is so high that coagulation process takes place, which reduces the particle number density to a basically dynamic equilibrium between the increasing factor (nucleation) and decreasing factor (coagulation) of particle number density. Although coagulation is not the dominant process in the four studied cases, it is shown in Fig. 14 that once the Re_j number is larger than 4800, the normalized particle number density increases due to the delay of turbulent mixing at high injection velocity (Garrick, 2015). As for the case with Re_j number of 12800, the low particle number density near the outlet of the aerosol reactor may be caused by the dead zone between the second and the third partitions of the aerosol reactor where those particles are trapped.

FIG.14. Normalized particle number density for simultaneous coagulation, nucleation and growth in turbulent flows.

More detailed information about computational accuracy and efficiency of the present modified CFD-MC method in Section S4 of the online SI file of this paper.

5. Conclusions

Typical simultaneous aerosol dynamic processes (i.e., coagulation, nucleation and growth) are widely encountered in turbulent flows. They are investigated with the present modified Lagrangian PDF approach based CFD-Monte Carlo method. The effect of Re_j number on the interactions between turbulence and aerosol dynamics is fully studied. The results reveal the significant impact of Re_j number on both single aerosol process (e.g. coagulation) and simultaneous competitive aerosol dynamic processes in turbulent flows. This newly modified CFD-Monte Carlo/PDF method renders an efficient method to deal with the interactions between turbulence and aerosol dynamics. The full PSD of aerosol particles is readily obtained. The enhancing effect of turbulence on coagulation is demonstrated by comparison of laminar coagulation and turbulent coagulation. Further study of the effect of turbulence on the PSDs of simultaneous aerosol dynamics reveals the competition between aerosol dynamic processes, which also has significant impact on the final PSD of particles. For simultaneous complex aerosol dynamics in turbulent flows, turbulence has an effect of broadening the PSD.

6. Acknowledgements

This work was supported by grants from the research studentship, Central Research Grant (Project No. G-YBF5) and Mechanical Engineering Department of The Hong Kong Polytechnic University. Last but not least, the financial support from the National Natural Science Foundation of China (Project No. 11572274) was also greatly appreciated for allowing the authors' further development and extension of this coupled CFD-Monte Carlo method in the study of aerosol dynamics.

References

Akridis, P., Rigopoulos, S. (2015). Modelling of soot formation in a laminar coflow non-premixed flame with a detailed CFD-population balance model. Procedia Engineering 102: 1274-1283.

Akroyd, J., Smith, A. J., Shirley, R., McGlashan, L. R., Kraft, M. (2011). A coupled CFD-population balance approach for nanoparticle synthesis in turbulent reacting flows. Chemical Engineering Science 66: 3792-3805.

Amokrane, A., Maass, S., Lamadie, F., Puel, F., Charton, S. (2016). On droplets size distribution in a pulsed column. Part I: In-situ measurements and corresponding CFD-PBE simulations. Chemical Engineering Journal 296: 366-376.

Balachandar, S., Eaton, J. K. (2010). Turbulent dispersed multiphase flow. Annual Review of Fluid Mechanics 42: 111-133.

Calvo, A. I., Alves, C., Castro, A., Pont, V., Vicente, A. M., Fraile, R. (2013). Research on aerosol sources and chemical composition: past, current and emerging issues. Atmospheric Research 120: 1-28.

Cenker, E., Bruneaux, G., Pickett, L., Schulz, C. (2013). Study of soot formation and oxidation in the engine combustion network (ECN), spray a: Effects of ambient temperature and oxygen concentration. SAE International Journal of Engines 6: 352-365.

Chan, T. L., Cheng, X. B. (2007). Numerical modeling and experimental study of combustion and soot formation in a direct injection diesel engine. Energy & Fuels 21: 1483-1492.

Chan, T. L., Liu, Y.H., Chan, C.K. (2010). Direct quadrature method of moments for the exhaust particle formation and evolution in the wake of the studied ground vehicle. Journal of Aerosol Science 41: 553-568.

Consalvi, J. L., Nmira, F. (2016). Transported scalar PDF modeling of oxygen-enriched turbulent jet diffusion flames: Soot production and radiative heat transfer. Fuel 178: 37-48.

Di Veroli, G.., Rigopoulos S. (2010). Modeling of turbulent precipitation: A transported population balance-PDF method. AIChE journal 56: 878-892.

Di Veroli, G.., Rigopoulos, S. (2011). Modeling of aerosol formation in a turbulent jet with the transported population balance equation-probability density function approach. Physics of Fluids 23: 043305.

Efendiev, Y. (2004). Modelling and simulation of multi- component aerosol dynamics. Computational & Applied Mathematics 23: 401-423.

Fox, R. O. (2003). Computational Models for Turbulent Reacting Flows. Cambridge University Press, Cambridge.

Friedlander, S. (2000). Smoke, Dust and Haze: Fundamentals of Aerosol Dynamics. Second ed. Oxford University Press, Oxford.

Garrick, S. C. (2015). Growth mechanisms of nanostructured Titania in turbulent reacting flows. Journal of Nanotechnology 2015, Article ID 642014: 1-10.

Geng, J., Park, H., Sajo, E. (2013). Simulation of aerosol coagulation and deposition under multiple flow regimes with arbitrary computational precision. Aerosol Science and Technology 47: 530-542.

Hounslow, M. J., Ryall, R. L., Marshall, V. R. (1988). A discretized population balance for nucleation, growth, and aggregation. AIChE Journal 34: 1821-1832.

Jaishree, J., Haworth, D. C. (2012). Comparisons of Lagrangian and Eulerian PDF methods in simulations of non-premixed turbulent jet flames with moderate-to-strong turbulence-chemistry interactions. Combustion Theory and Modelling 16: 435-463

Kruis, F. E., Wei, J. M., van der Zwaag, T., Haep, S. (2012). Computational fluid dynamics based stochastic aerosol modelling: combination of a cell-based weighted random walk method and a constant-number Monte-Carlo method for aerosol dynamics. Chemical Engineering Science 70: 109-120.

Kumar, P., Ketzel, M., Vardoulakis, S., Pirjola, L., Britter, R. (2011). Dynamics and dispersion modelling of nanoparticles from road traffic in the urban atmospheric environment-a review. Journal of Aerosol Science 42: 580-603.

Liu, S. Y., Chan, T. L., Zhou, K. (2015). A new stochastically weighted operator splitting Monte Carlo method for particle-fluid systems. ASME-ATI-UIT 2015 Conference on Thermal Energy Systems: Production, Storage, Utilization and the Environment (In Session: Computational Thermal-fluid Dynamics), May 17-20, Naples, Italy.

Liu, S. Y., Chan, T. L. (2016). A stochastically weighted operator splitting Monte Carlo (SWOSMC) method for the numerical simulation of complex aerosol dynamic processes. International Journal of Numerical Methods for Heat & Fluid Flow, Accepted for publication.

Lundgren, T. S. (1967). Distribution functions in the statistical theory of turbulence. Physics of Fluids 10: 969-975.

Meyer, D. W. (2010). A new particle interaction mixing model for turbulent dispersion and turbulent reactive flows. Physics of Fluids 22: 035103.

Mobus, H., Gerlinger, P., Brüggemann, D. (2001). Comparison of Eulerian and Lagrangian Monte Carlo PDF methods for turbulent diffusion flames. Combustion and Flame 124: 519-534.

Pang, K. M., Karvounis, N., Walther, J. H., Schramm, J. (2016). Numerical investigation of soot formation and oxidation processes under large two-stroke marine diesel engine-like conditions using integrated CFD-chemical kinetics. Applied Energy 169: 874-887.

Pesmazoglou, I., Kempf, A. M., Navarro-Martinez, S. (2014). Aerosol nucleation in a turbulent jet using Large Eddy Simulations. Chemical Engineering Science 116: 383-397.

Pesmazoglou, I., Kempf, A. M., Navarro-Martinez, S. (2016). Stochastic modelling of particle aggregation. International Journal of Multiphase Flow 80: 118-130.

Pope, S. B. (1981). A Monte Carlo method for PDF equations of turbulent reactive flow. Combustion Science and Technology 25: 159-174.

Pope, S. B. (1985). PDF methods for turbulent reactive flows. Progress in Energy and Combustion Science 11: 119-192.

Pope, S. B., Tirunagari, R. (2014). Advances in probability density function methods for turbulent reactive flows. In Proceedings of the Nineteenth Australasian Fluid Mechanics Conference, RMIT University, Melbourne.

Ramkrishna, D. (2000). Population balances: Theory and applications to particulate systems in engineering. Academic press, San Diego.

Reade, W. C., Collins, L. R. (2000). A numerical study of the particle size distribution of an aerosol undergoing turbulent coagulation. Journal of Fluid Mechanics 415: 45-64.

Rigopoulos, S. (2007). PDF method for population balance in turbulent reactive flow. Chemical Engineering Science 62: 6865-6878.

Rigopoulos, S., Jones, A.G. (2003). Finite-element scheme for solution of the dynamic population balance equation. AIChE Journal 49: 1127-1139.

Sabel'nikov, V., Soulard, O. (2005). Rapidly decorrelating velocity-field model as a tool for solving one-point Fokker-Planck equations for probability density functions of turbulent reactive scalars. Physical Review E 72: 016301.

Saffman, P. G., Turner, J.S. (1956). On the collision of drops in turbulent clouds. Journal of Fluid Mechanics 1: 16-30.

Valino, L. (1998). Field Monte Carlo formulation for calculating the probability density function of a single scalar in a turbulent flow. Flow Turbulence and Combustion 60: 157-172.

Yu, M. Z., Lin, J. Z., Chan, T. L. (2008). Effect of precursor loading on non-spherical TiO_2 nanoparticle synthesis in a diffusion flame reactor. Chemical Engineering Science 63: 2317-2329.

Yu, M. Z., Lin, J. Z., Chan, T. L. (2009). Numerical simulation for nucleated vehicle exhaust particulate matters via the TEMOM/LES method. International Journal of Modern Physics C 20: 399-421.

Yu, M. Z., Chan, T. L. (2015). A bimodal moment method model for submicron fractal-like agglomerates undergoing Brownian coagulation. Journal of Aerosol Science 88: 19-34.

Zhang, Z., Chen, Q. (2007). Comparison of the Eulerian and Lagrangian methods for predicting particle transport in enclosed spaces. Atmospheric Environment 41: 5236-5248.

Zhao, H. B., Zheng, C. G. (2013). A population balance-Monte Carlo method for particle coagulation in spatially inhomogeneous systems. Computers & Fluids 71: 196-207.

Zhou, K., Chan, T. L. (2011). Simulation of homogeneous particle nucleation in a free turbulent jet. Aerosol Science and Technology 45: 973-987.

Zhou, K., Chan, T. L. (2014). Analytical approximation schemes for mean nucleation rate in turbulent flows. Aerosol Science and Technology 48: 459-466.

Zhou, K., He, Z. (2014). Monte Carlo simulation of aerosol evolution in a planar mixing layer. International Journal of Numerical Methods for Heat & Fluid Flow 24: 1769-1781.

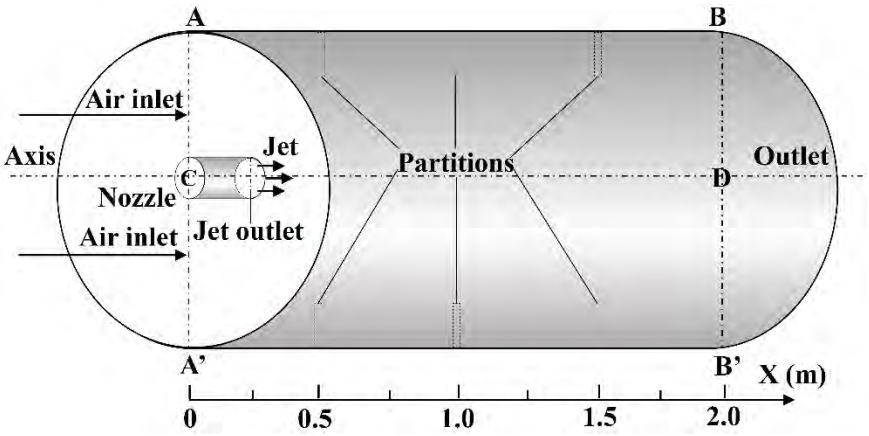

FIG.1. Three-dimensional schematic configuration of a cylindrical aerosol reactor (Two-dimensional axisymmetric grid is generated in the rectangular domain ABCD, not in scale).

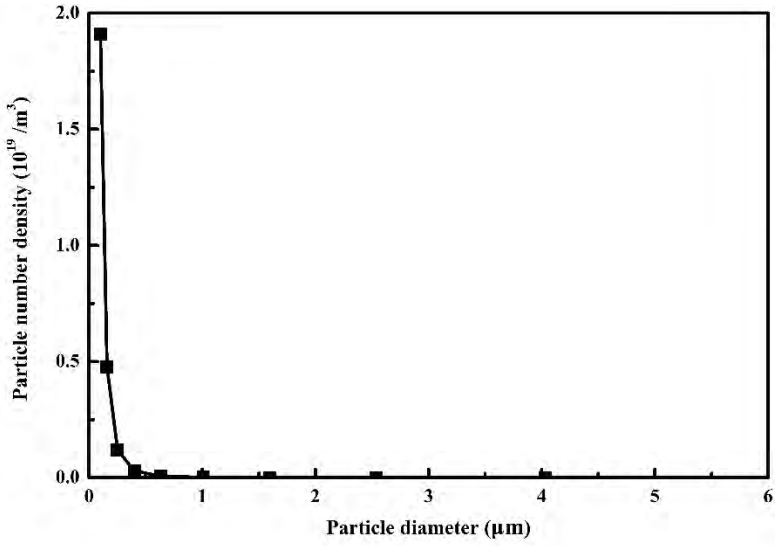

FIG. 2. Initial PSD before entering the aerosol reactor.

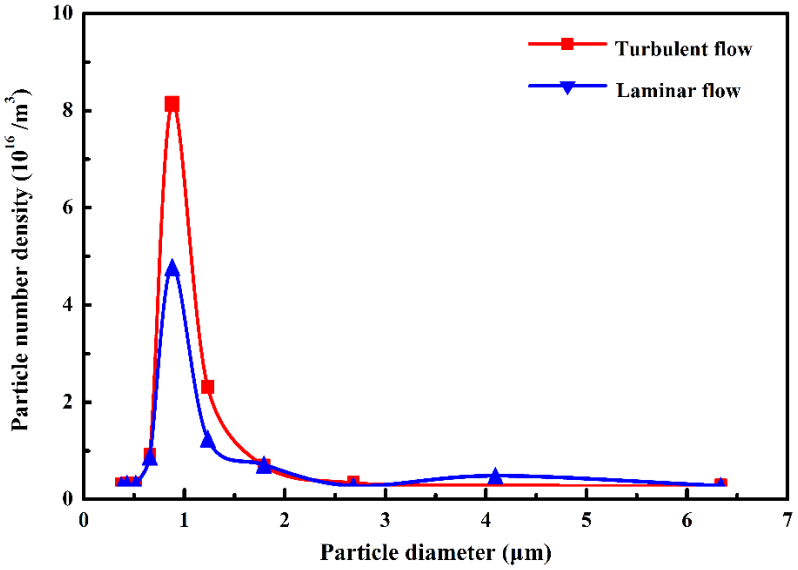

FIG. 3. PSD in laminar and turbulent coagulation.

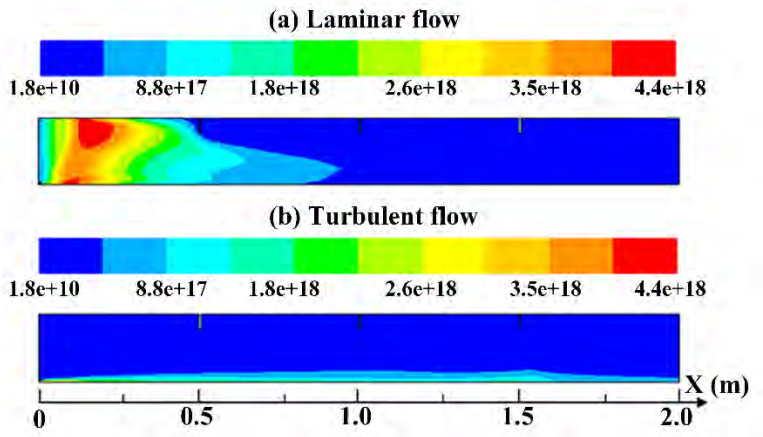

FIG. 4. Particle number density (#/m^3) contour in laminar and turbulent coagulation.

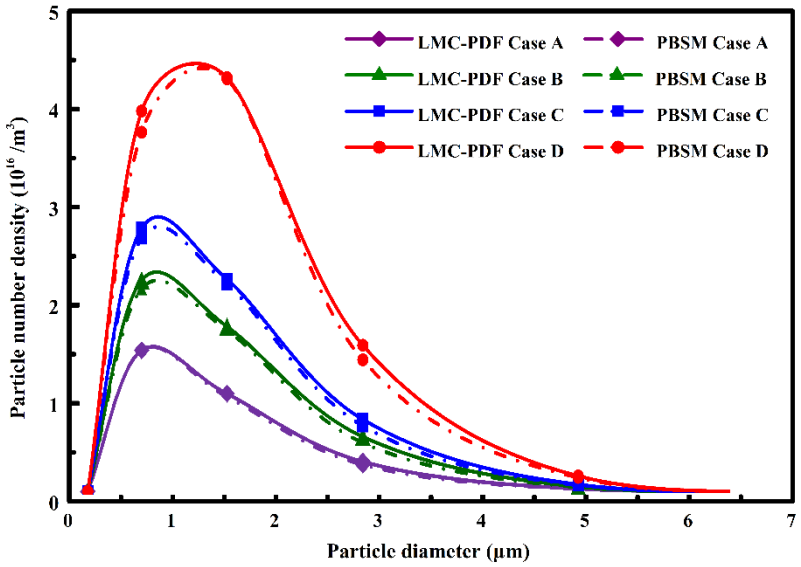

FIG. 5. PSD in turbulent coagulation: Case A, Re_j=3200; Case B, Re_j=4800; Case C, Re_j=6400; Case D, Re_j=12800 (The PBSM results are obtained based on the method proposed by Hounslow et al., 1988).

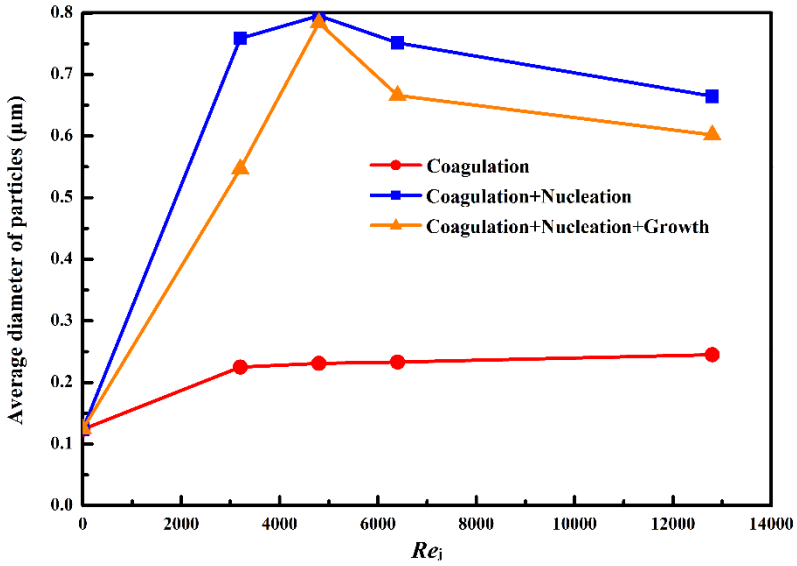

FIG. 6. Average diameter of particles for different aerosol dynamic processes in turbulent flows.

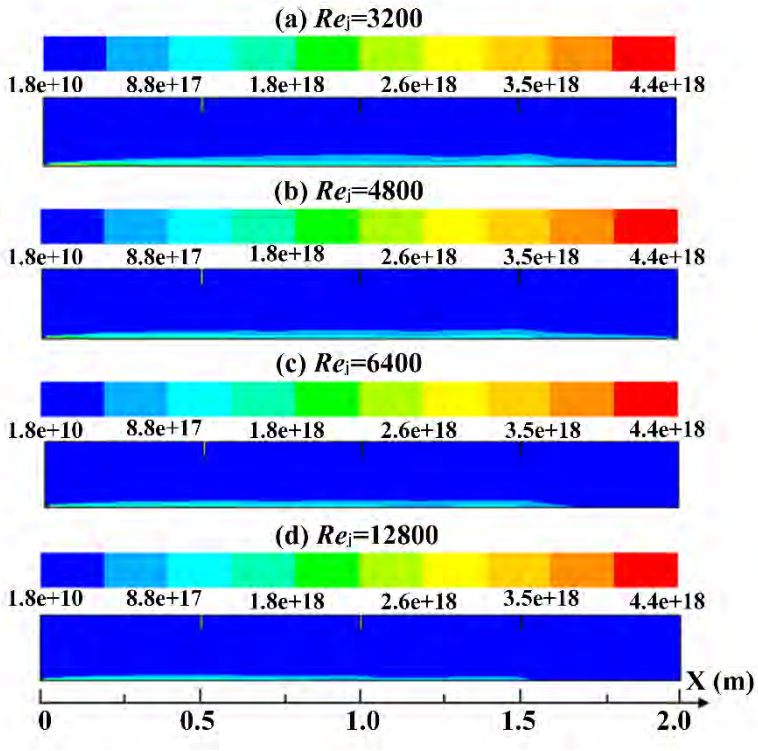

FIG. 7. Particle number density (#/m^3) contour in turbulent coagulation.

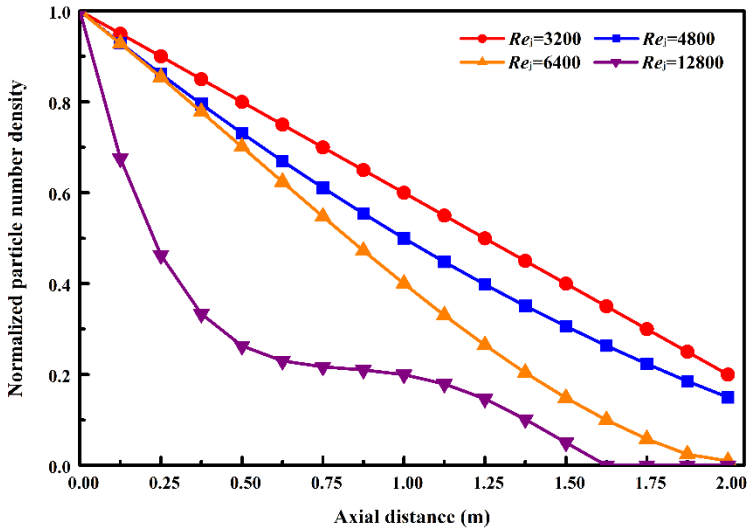

FIG. 8. Normalized particle number density in turbulent coagulation.

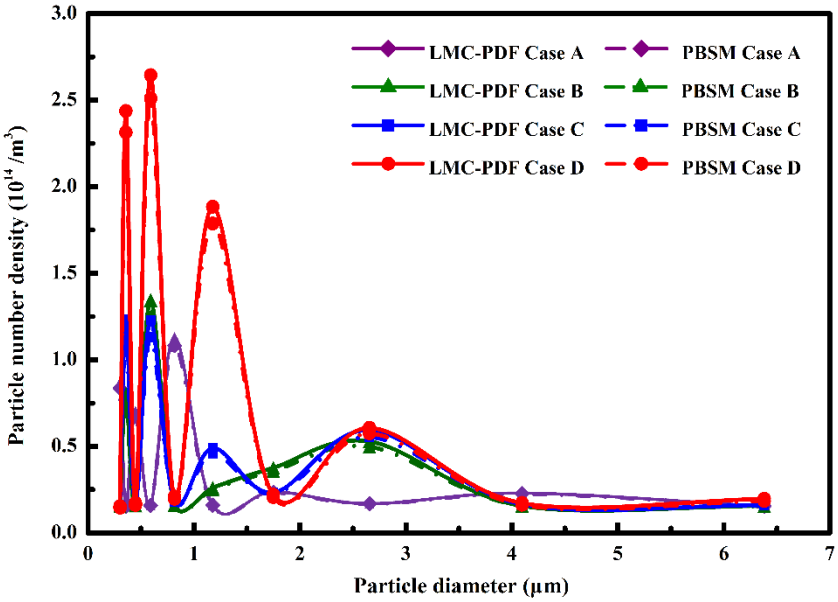

FIG. 9. PSD for simultaneous coagulation and nucleation in turbulent flows: Case A, Re_j=3200; Case B, Re_j=4800; Case C, Re_j=6400; Case D, Re_j=12800 (The PBSM results are obtained based on the method proposed by Hounslow et al., 1988).

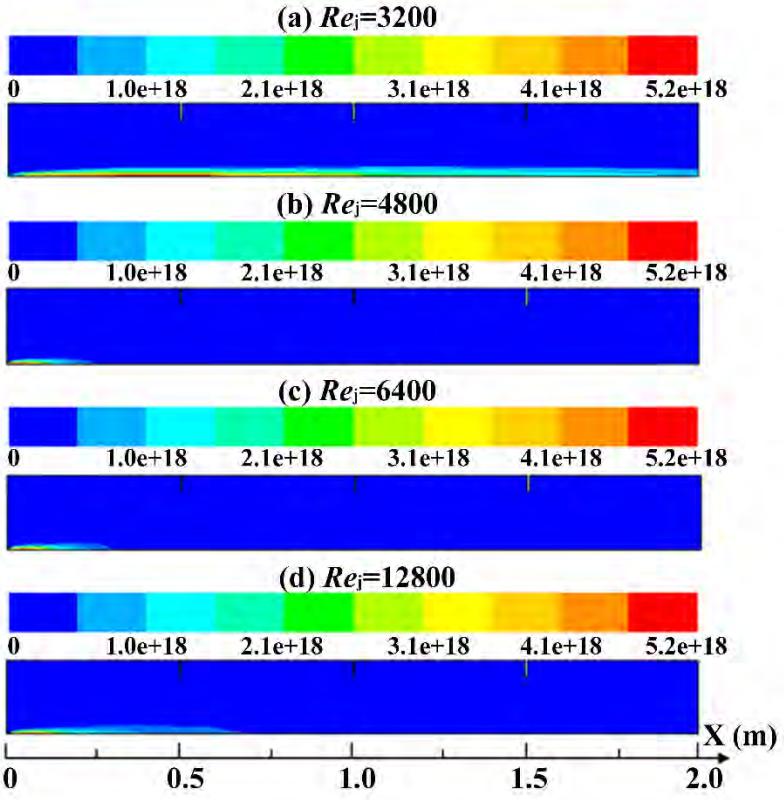

FIG. 10. Particle number density (#/m^3) contour for simultaneous coagulation and nucleation in turbulent flows.

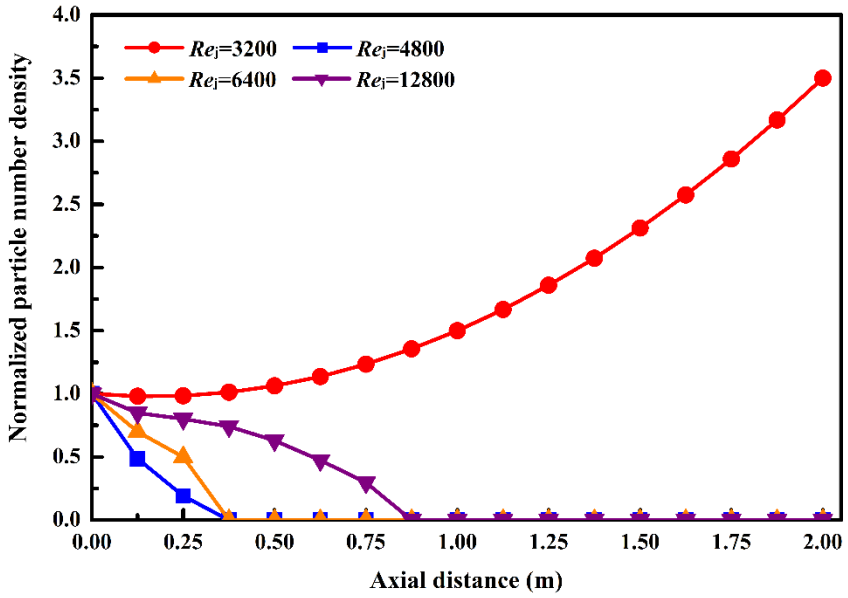

FIG. 11. Normalized particle number density for simultaneous coagulation and nucleation in turbulent flows.

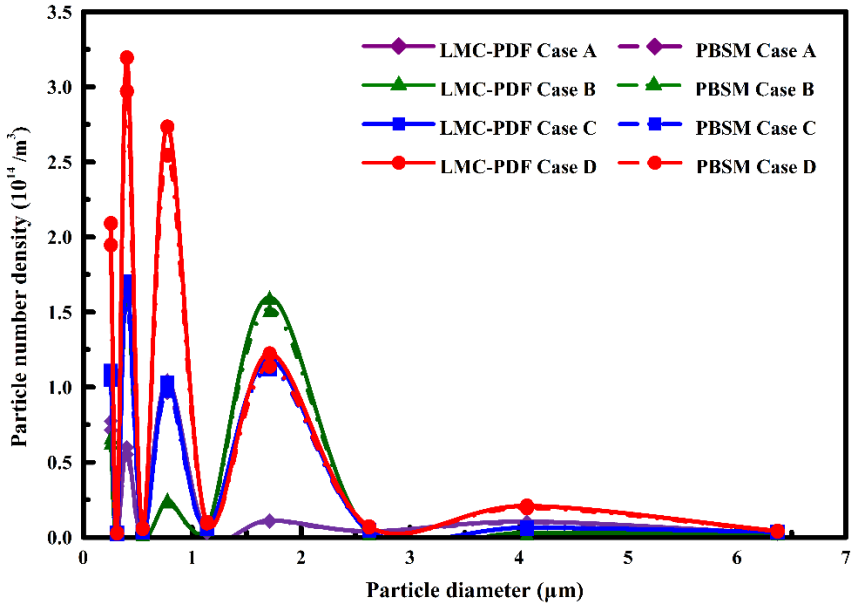

FIG. 12. PSD for simultaneous coagulation, nucleation and growth in turbulent flows: Case A, Re_j=3200; Case B, Re_j=4800; Case C, Re_j=6400; Case D, Re_j=12800 (The PBSM results are obtained based on the method proposed by Hounslow et al., 1988).

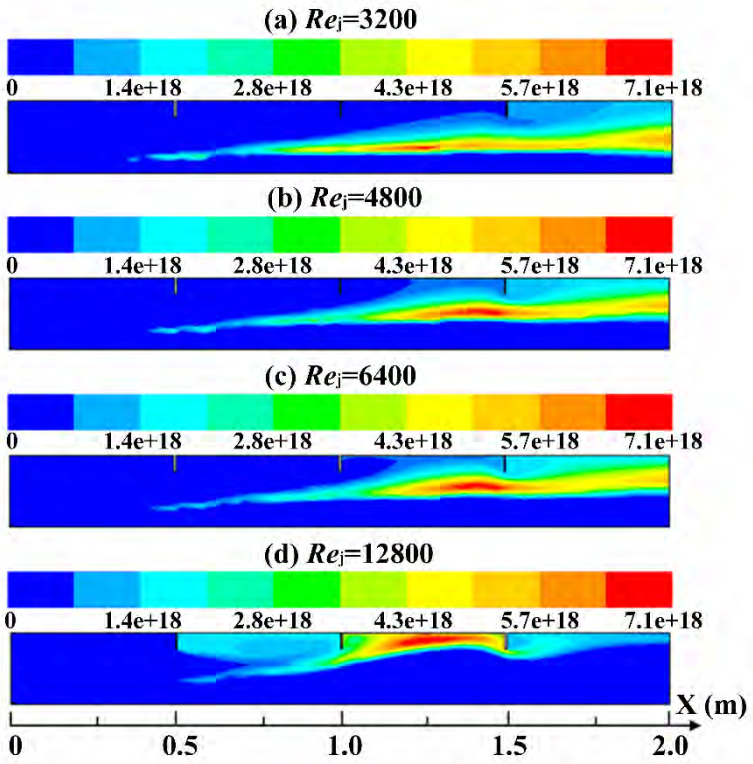

FIG. 13. Particle number density (#/m^3) contour for simultaneous coagulation, nucleation and growth in turbulent flows.

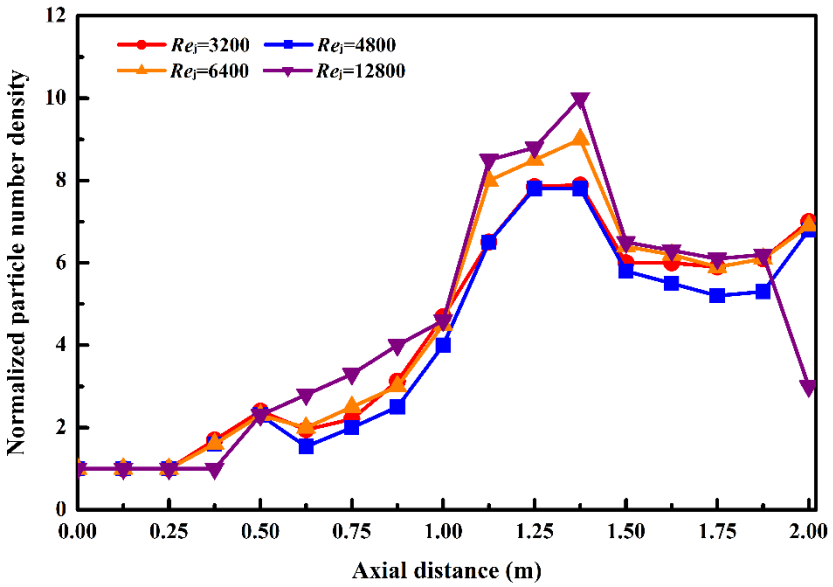

FIG.14. Normalized particle number density for simultaneous coagulation, nucleation and growth in turbulent flows.

Table 1. Simulation parameters for aerosol dynamics in turbulent flows.

Particulate phase	Potassium chloride (KCl)
Particle density (kg/m^3)	1980
Initial particle size range (μm)	0.1−6.4
Injection velocity of the jet (m/s)	10−40
Corresponding Re_j of the jet	3200−12800
Velocity of continuous phase (m/s)	0.5
Coagulation model	Turbulent kernel (Saffman and Turner, 1956)
Nucleation rate (#/m^3·s)	7.5×10^6
Growth rate (m/s)	6.2×10^{-11}
The number of cells in the computational domain	8112
The number of simulation particles per cell	30
Turbulence model	k-ε model